Chemical Engineering Science 81 (2012) 191–201

Contents lists available at SciVerse ScienceDirect

Chemical Engineering Science

journal homepage: www.elsevier.com/locate/ces

Surface morphology control of Transparent Conducting Oxide layers for improved light trapping using wafer grating and feedback control

Jianqiao Huang [a], Gerassimos Orkoulas [a], Panagiotis D. Christofides [a,b,*]

[a] Department of Chemical and Biomolecular Engineering, University of California, Los Angeles, CA 90095, USA
[b] Department of Electrical Engineering, University of California, Los Angeles, CA 90095, USA

HIGHLIGHTS

- Simulation of the evolution of film surface morphology using wafer grating.
- Investigation of the impact of wafer grating parameters on film surface morphology.
- Integration of wafer grating and feedback control.
- Manufacturing of thin films with desired surface morphology.

ARTICLE INFO

Article history:
Received 12 April 2012
Received in revised form
5 July 2012
Accepted 10 July 2012
Available online 20 July 2012

Keywords:
Process control
Process simulation
Thin films
Solar cells
Process design
Wafer grating

ABSTRACT

This work first introduces a kinetic Monte-Carlo simulation model for a two-species thin film deposition process on a grated (patterned) wafer, and then utilizes a model predictive controller, which manipulates a spatially distributed deposition rate, to produce thin films whose surface morphology has a structure that improves light trapping. This approach to thin film surface morphology control can be applied to many deposition processes, and in particular, in the context of Transparent Conducting Oxide (TCO) thin film manufacturing processes used in thin film solar cells where it is desirable to produce thin films with precisely tailored surface morphology. Specifically, a two species thin film deposition process involving atom adsorption, surface relaxation and surface migration is considered and is modeled on a large-scale lattice (lattice size=40,000) via kinetic Monte-Carlo methods and aggregate surface roughness and slope are used to describe the surface morphology. Subsequently, multiple sets of simulations are carried out to understand the process dynamics dependence on wafer grating parameters, such as magnitude and period of grating, and other process parameters, such as temperature and deposition rate. From these simulations, it is concluded that a spatially distributed deposition rate profile is necessary to be utilized across the lattice in order to induce desirable surface morphology at light wavelength spatial scales that lead to desired thin film solar cell performance. Then, an Edwards–Wilkinson-type equation is utilized to predict the surface evolution and forms the basis for the design of a predictive feedback controller. The model parameters of the Edwards–Wilkinson equation are identified from kinetic Monte-Carlo open-loop simulations. Analytical solutions of the expected surface roughness and surface slope at the visible light wavelength spatial scale are obtained by solving the Edwards–Wilkinson equation and are used in the predictive controller formulation and in the control action calculation. The controller is applied to the kinetic Monte-Carlo simulation of the deposition process taking place on a sinusoidal grated wafer. Simulation results demonstrate that the proposed controller, wafer grating and patterned actuator design successfully regulate aggregate surface roughness and slope to desirable set-point values at the end of the deposition.

1. Introduction

Thin film solar cell technology is playing an increasingly important role in the overall solar cell market (see, for example, Green, 2007; van Sark et al., 2007) owing to the potential of improving light conversion efficiencies (currently on the order of 10% for production modules). The Transparent Conducting Oxide (TCO) layer, which consists of zinc oxide (ZnO) and aluminum (Al), is an important component of thin film solar cells and has a crucial influence on the performance of thin film based solar cell systems (see, for example, Krč and Zeman, 2003; Gospodyn and Sit, 2006). In addition to investigating the performance with respect to light conversion efficiency and long-term stability of

* Corresponding author at: Department of Chemical and Biomolecular Engineering, University of California, Los Angeles, CA 90095, USA. Tel.: +1 310 794 1015; fax: +1 310 206 4107.
E-mail address: pdc@seas.ucla.edu (P.D. Christofides).

0009-2509/$ - see front matter © 2012 Elsevier Ltd. All rights reserved.
http://dx.doi.org/10.1016/j.ces.2012.07.011

an array of materials, thin film solar cell technology stands to benefit from optimal thin film manufacturing (deposition) control strategies that produce thin films with desired light trapping properties. Specifically, extensive research has demonstrated that the surface morphology at the interface, which is characterized by surface roughness and slope, directly influences the efficiency of thin-film silicon solar cells (see, for example, Gospodyn and Sit, 2006; Krč and Zeman, 2003; Zeman and Vanswaaij, 2000; Poruba et al., 2000; Muller and Rech, 2004; Rowlands et al., 2004). Shaping the surface morphology of the TCO layer at the thin film deposition stage is therefore critical in order to maximize the amount of light energy converted to electrical energy. In the solar cell industry, wafer grating, which means using suitably patterned wafers for solar panel manufacturing, is the most commonly used method to introduce rough surfaces on TCO layers (Li et al., 2012; Ferry et al., 2011; Chen et al., 2010; Campa et al., 2010), and different grating methods, for example, line grating and sinusoidal grating, can be used to shape the wafer surface (Naqavi et al., 2011; Madzharov et al., 2011; Chong et al., 2012). However, the wafer grating takes place before the deposition of the TCO layer and it is not possible to precisely control the surface morphology during the TCO thin film growth process by only using wafer grating. Therefore, a spatially distributed deposition rate profile, which has been proved to be effective in shaping surface morphology in thin films (Huang et al., 2011, 2012b), is combined with wafer grating in this work to provide on-line and precise control of TCO surface morphology for improved TCO light trapping performance.

Extensive efforts have been made in recent years on the modeling and model-based feedback control of thin film deposition processes in the context of improving solar cell performance (Krč and Zeman, 2003; Huang et al., 2010b, 2011). Thin film growth processes are usually modeled via kinetic Monte-Carlo (kMC) methods and stochastic partial differential equations (Huang et al., 2012a). Since kMC models are not available in closed form and cannot be readily used for feedback control design and system-level analysis, stochastic differential equation (SDE) models (whose parameters are computed from kMC model data) have been used as the basis for the design of feedback controllers to regulate thin film surface roughness (e.g., Christofides et al., 2008; Ni and Christofides, 2005; Varshney and Armaou, 2005, 2006; Hu et al., 2009a), film porosity (Hu et al., 2009a,b), and film thickness. In an attempt to manufacture thin film solar cells with optimal light conversion efficiencies, we previously conducted research on the modeling and control of silicon thin film surface morphology to optimize thin film light trapping properties (Huang et al., 2011, 2012b), and of TCO layer deposition using spatially distributed deposition rate profiles (Huang et al., 2012a); the use of wafer grating to shape surface morphology has not, however, been previously studied.

Motivated by the above considerations, in the present paper, we focus on the application of microscopic modeling and analysis of a TCO thin film deposition process on a sinusoidal grated wafer, and model predictive control is utilized to control the surface morphology to desired values. To demonstrate the approach, we focus on a two species thin film deposition process using a grated initial lattice, which is modeled via kinetic Monte-Carlo simulation. The initial lattice is defined based on a sinusoidal function with proper magnitude ($M=100$ layers) and five sine waves are placed across the lattice. Since a square lattice is used in the model, the initial heights of all the sites are rounded to the nearest lattice site. Different deposition mechanisms are utilized for each component, ZnO and Al. Specifically, a random deposition with surface relaxation (RDSR) mechanism is used for Al and a deposition/migration mechanism is used for ZnO (Huang et al., 2010a). Since a large-lattice kinetic Monte-Carlo model cannot be used as the basis for controller design and real-time controller calculations, an Edwards–Wilkinson-type equation is used to model the surface evolution and to form the basis for feedback controller design within a model predictive control framework. The cost function of the predictive controller involves penalties on both surface roughness and slope, following Huang et al. (2012b). Extensive simulation studies demonstrate that the proposed controller and patterned actuator design successfully regulate surface roughness and slope at visible light wavelength spatial scales to desired set-point values at the end of the deposition.

2. Two species thin film deposition process description and modeling

In this section, a one-dimensional solid-on-solid (SOS) on-lattice model is used to simulate the two species thin film deposition process via a kinetic Monte-Carlo method, which includes three microscopic processes: an adsorption process, in which particles are incorporated onto the film from the gas phase, a migration process and a surface relaxation process, in which surface particles move to adjacent sites (Levine et al., 1998; Levine and Clancy, 2000; Wang and Clancy, 2001; Yang et al., 1997). In this work, a square lattice is selected to represent the structure of the film and a sinusoidal grated wafer is used to initialize the deposition lattice, as shown in Fig. 1. The initial heights of all the particle sites are calculated as follows:

$$h_0(x) \approx M \cdot \sin\left(\frac{2\pi x}{p}\right) + M, \quad x \in [0, L] \tag{1}$$

All particles are modeled as identical hard spheres and the centers of the particles deposited on the film are located on the lattice sites. If the initial heights of the particles, $h_0(x)$, are not integers, they are approximated with the closest integers to satisfy the assumptions of on-lattice models. The diameter of the particles equals the distance between two neighboring sites. The width of the lattice is fixed so that the lattice contains a fixed number of sites in the lateral direction. The new particles are always deposited from the top side of the lattice with vertical incidence; see Fig. 1. Particle deposition results in film growth in the direction normal to the lateral direction. The direction normal to the lateral direction is thus designated as the growth direction. The number of sites in the lateral direction is defined as the lattice size and is denoted by L. Periodic boundary

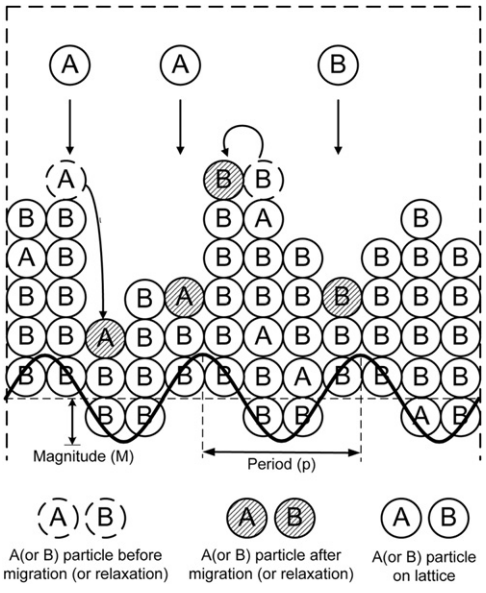

Fig. 1. Two species thin film growth process on a solid-on-solid one-dimensional square lattice with sinusoidal grated wafer.

conditions (PBCs) are applied at the edges of the lattice in the lateral direction. We note that the size of the atomic radii for Zn is 0.135 nm, for O is 0.06 nm and for Al is 0.125 nm. Therefore, the overall particle sizes for ZnO or Al are comparable at a first approximation and thus, the above set-up of the lattice is reasonable from an atomic size point of view.

The top particles of each column are defined as the surface particles and the positions of the centers of all surface particles form the surface height profile. The number of nearest neighbors of a surface particle ranges from zero to two. A surface particle with zero nearest neighbors is possible to move to one of its adjacent columns with equal probability. A surface particle with one nearest neighbor is possible to move to its adjacent column with lower height. A surface particle with two nearest neighbors cannot move. Particles that are not on the film surface cannot move.

The overall deposition rate, w, is expressed in units of layers per second and is a superposition of two components, ZnO deposition rate w_1 and Al deposition rate w_2 ($w=w_1+w_2$). The deposition ratio between ZnO and Al is 24:1 (Das et al., 2005). Different deposition mechanisms are used for each component. Random deposition with surface relaxation (RDSR) mechanism is used for Al and deposition/migration mechanism is used for ZnO. For a description and comparison between these two mechanisms, refer to Huang et al. (2012a). The migration rate (probability) follows an Arrhenius-type law with a pre-calculated activation energy barrier that depends on the local environment of the particle, i.e., the number of the nearest neighbors of the particle chosen for a migration event. The migration rate of the ith surface particle is calculated as follows:

$$r_m = v_0 \exp\left(-\frac{E_s + n_i E_n}{k_B T}\right) \tag{2}$$

where v_0 denotes the pre-exponential factor, n_i is the number of the nearest neighbors of the ith particle and can take the values of 0 and 1, (r_m is zero when $n_i=2$ since in the one-dimensional lattice this surface particle is fully surrounded by other particles and cannot migrate), k_B is the Boltzmann's constant, E_s is the contribution to the activation energy barrier from the site itself, and E_n is the contribution to the activation energy barrier from each nearest neighbor. In this work, $E_s=3.4$ eV and E_n is assumed to be zero (Moller and Palumbo, 2001). T is the substrate temperature of the thin film and in this work $T=800$ K (Mirica et al., 2004). Since the film is thin, the temperature is assumed to be uniform throughout the film. For a detailed description and study of these models, refer to Huang et al. (2010a).

2.1. Surface morphology at atomic level

Thin film surface morphology, which includes surface roughness and slope, is a very important surface property influencing the light properties of TCO thin films. Surface roughness is defined as the root-mean-square (RMS) of the surface height profile as follows (Huang et al., 2010b):

$$r = \left[\frac{1}{L}\sum_{i=1}^{L}(h_i - \overline{h})^2\right]^{1/2} \tag{3}$$

where r denotes surface roughness, h_i ($i=1,2,\ldots,L$), is the surface height at the ith position in the unit of layer, L denotes the lattice size, and the surface mean height is given by $\overline{h} = (1/L)\sum_{i=1}^{L} h_i$.

In addition to surface roughness, the surface mean slope is defined as the RMS of the surface gradient profile as follows (Huang et al., 2010b):

$$m = \left[\frac{1}{L}\sum_{i=1}^{L} h_{s,i}^2\right]^{1/2} \tag{4}$$

where m denotes the RMS slope and $h_{s,i}$ is the surface slope at the ith lattice site, which is a dimensionless variable. The surface slope, $h_{s,i}$ is computed as follows:

$$h_{s,i} = \frac{h_{i+1} - h_i}{1} \tag{5}$$

2.2. Aggregate surface morphology and spatial deposition rate profile

In the context of TCO manufacturing for improved solar cell performance, the roughness and slope should be calculated at a length scale that is comparable to the wave length of visible light. Thus, aggregate surface morphology should be used in this work and the aggregation length, Δ, is 400 (Huang et al., 2010b, 2011). Specifically, the aggregate surface morphology is computed similarly to the atomic surface morphology, but on the basis of the aggregate surface height profile, $h_{\Delta,i}$, which is defined as follows:

$$h_{\Delta,i} = (h_{i\Delta+1} + h_{i\Delta+2} + \cdots + h_{(i+1)\Delta})/\Delta, \quad i = 0,1,\ldots,L/\Delta - 1 \tag{6}$$

where $h_{\Delta,i}$ denotes the averaged surface height over the length scale of Δ sites, Δ denotes the aggregation size, i.e., the number of lattice sites used to calculate the aggregate surface height, and L/Δ denotes the number of aggregate sites of size Δ included in the spatial domain of the process. For the wavelength of visible light and silicon thin-film solar cells, the corresponding Δ is around 400; this follows from the fact that $0.3 \cdot 400 = 120$ nm, which is a length scale comparable to visible light wavelength (Huang et al., 2011); the same aggregation level is used for the TCO layer in this work. The definition of aggregate surface roughness and slope is given as follows:

$$r_\Delta = \left[\frac{1}{L/\Delta}\sum_{i=1}^{L/\Delta}(h_{\Delta,i} - \overline{h}_\Delta)^2\right]^{1/2}$$

$$m_\Delta = \left[\frac{1}{L/\Delta}\sum_{i=1}^{L/\Delta}\left(\frac{h_{\Delta,i} - h_{\Delta,i+1}}{\Delta}\right)^2\right]^{1/2} \tag{7}$$

To investigate the properties of aggregate roughness and slope in this model, multiple sets of simulations were carried out with different parameter values. First, simulations were carried out to investigate the surface morphology dependence on wafer grating parameters, specifically, magnitude (M) and period (P) of grating. As shown in Figs. 2 and 3, $W=5$ layer/s, $T=800$ K, $M=100$ layers and 1000 independent simulations were carried out to calculate the expected values of aggregate surface roughness and slope. It is

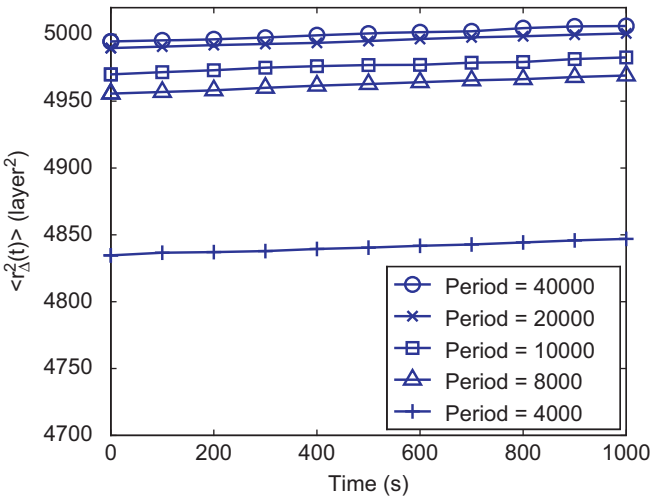

Fig. 2. Evolution of expected aggregate surface roughness with respect to time for different grating period lengths obtained from kMC simulations.

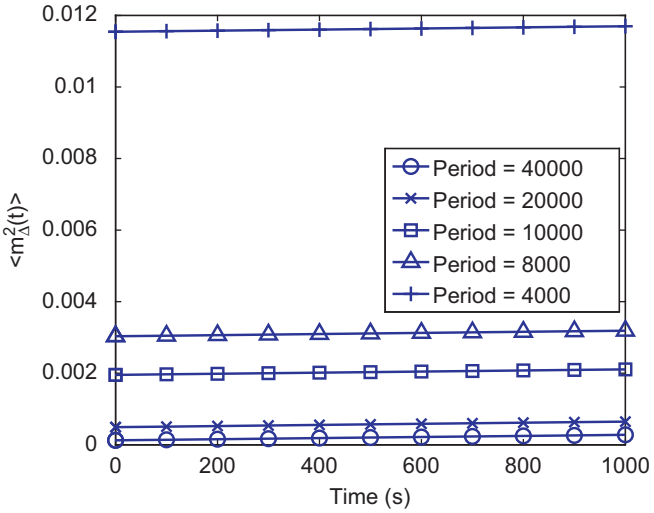

Fig. 3. Evolution of expected aggregate surface slope with respect to time for different grating period lengths obtained from kMC simulations.

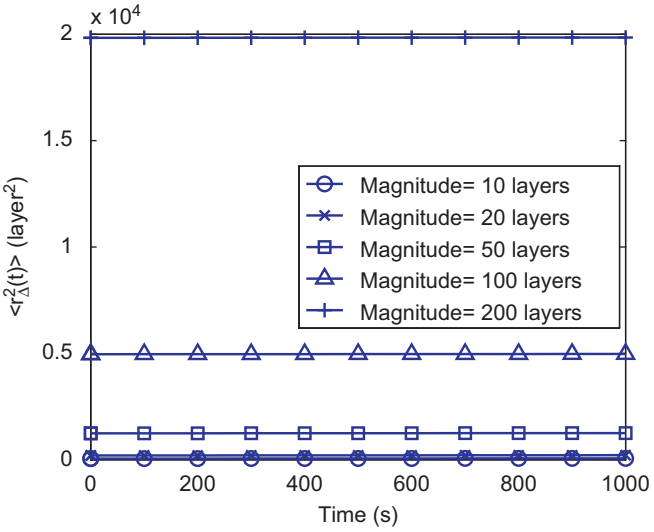

Fig. 4. Evolution of expected aggregate surface roughness with respect to time for different grating magnitudes obtained from kMC simulations.

clear that as the period, P, decreases from 40,000 to 4000, aggregate slope increases by two orders of magnitude while aggregate roughness decreases slightly. As shown in Figs. 4 and 5, with same T and W as in the previous simulation set and $P=8000$, as the grating magnitude increases, both aggregate roughness and slope increase dramatically. Subsequently, more simulations were carried out with the same wafer grating parameters, $P=8000$ and $M=100$ layers, but different T and W. From Figs. 6–9, we observe that both the temperature, T, and the uniform deposition rate, W, have very limited influence on aggregate roughness and slope. This is as expected since wafer grating influences the shape of the surface in a macroscopic way, while T and W influence the surface in a microscopic way via the deposition and migration rates and they are not strong enough to influence the shape of the surface within a practically meaningful deposition time. In order to induce large enough aggregate surface roughness and slope to precisely control the surface morphology on a sinusoidal grated wafer, a spatially non-uniform deposition rate profile is necessary for the purpose of optimizing thin film light trapping properties by the manipulation of film aggregate surface roughness and slope at length scales comparable to visible light wavelength (Huang et al., 2011). To this end,

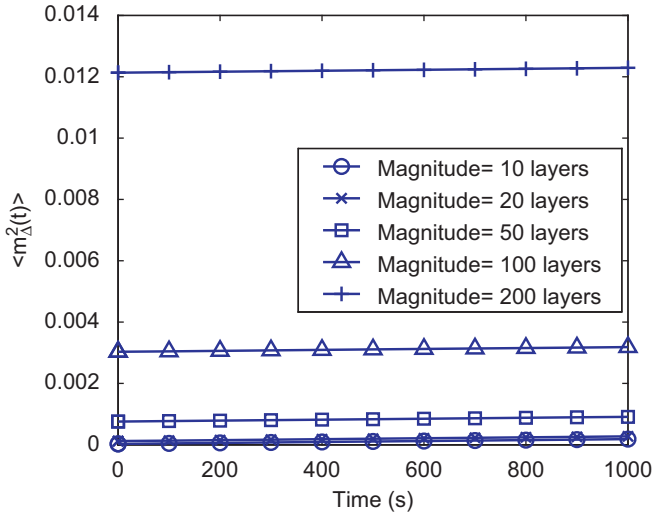

Fig. 5. Evolution of expected aggregate surface slope with respect to time for different grating magnitudes obtained from kMC simulations.

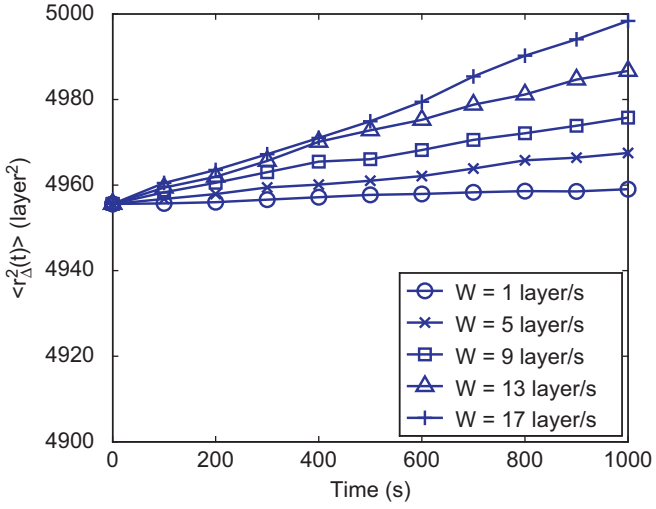

Fig. 6. Evolution of expected aggregate surface roughness with respect to time for different uniform deposition rates obtained from kMC simulations.

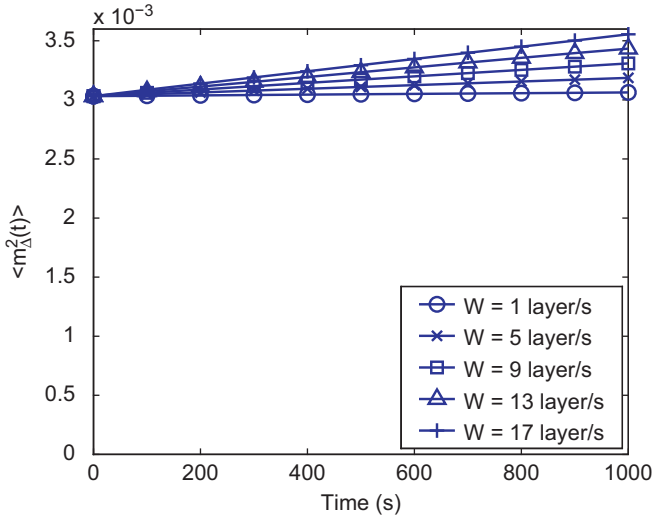

Fig. 7. Evolution of expected aggregate surface slope with respect to time for different uniform deposition rates obtained from kMC simulations.

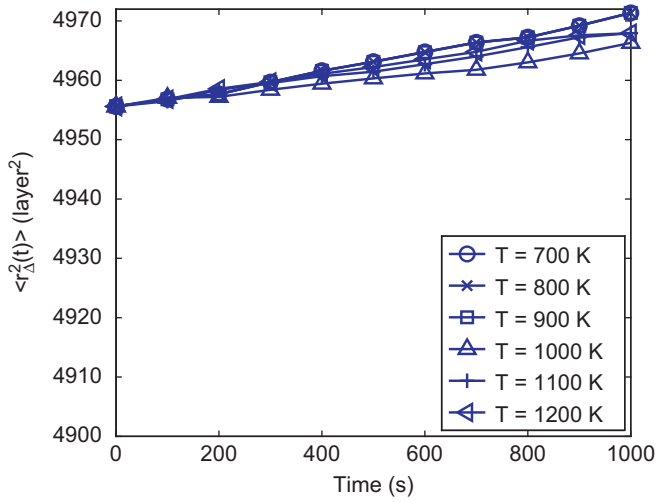

Fig. 8. Evolution of expected aggregate surface roughness with respect to time for different temperatures obtained from kMC simulations.

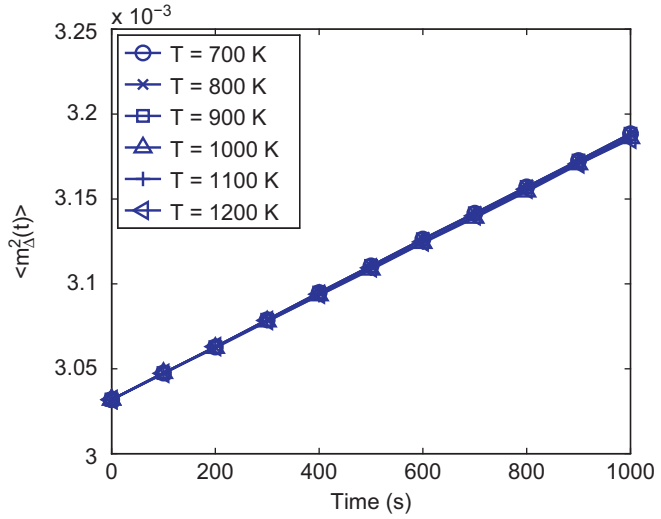

Fig. 9. Evolution of expected aggregate surface slope with respect to time for different temperatures obtained from kMC simulations.

a spatially patterned deposition rate profile is used in this work, which is defined as follows:

$$w_1(x) = w_{1,0} + A_1 \sin\left(\frac{2k\pi}{L}x\right), \quad A_1 \le w_{1,0}$$

$$w_2(x) = w_{2,0} + A_2 \sin\left(\frac{2k\pi}{L}x\right), \quad A_2 \le w_{2,0}$$

$$w(x) = w_1(x) + w_2(x)$$

$$w_0(x) = w_{1,0}(x) + w_{2,0}(x), \quad A = A_1 + A_2 \tag{8}$$

where x is a position along the lattice, $w_{1,0}$ and $w_{2,0}$ are the mean deposition rates, A_1 and A_2 are the magnitude of the patterned deposition profile, k is the number of sine waves along the entire lattice, and L is the lattice size. It is considered that $w_1 : w_2 = w_{1,0} : w_{2,0} = A_1 : A_2 = 24 : 1$.

The dynamics of aggregate surface morphology with patterned deposition rate profile is studied by carrying out a series of simulations at different mean deposition rates w_0 with $M=100$ layers, $P=8000$, $L=40{,}000$, $\Delta = 400$, $T=800$ K, $k=1$ and $A = 0.1w_0$. The evolution profiles for aggregate roughness and slope are shown in

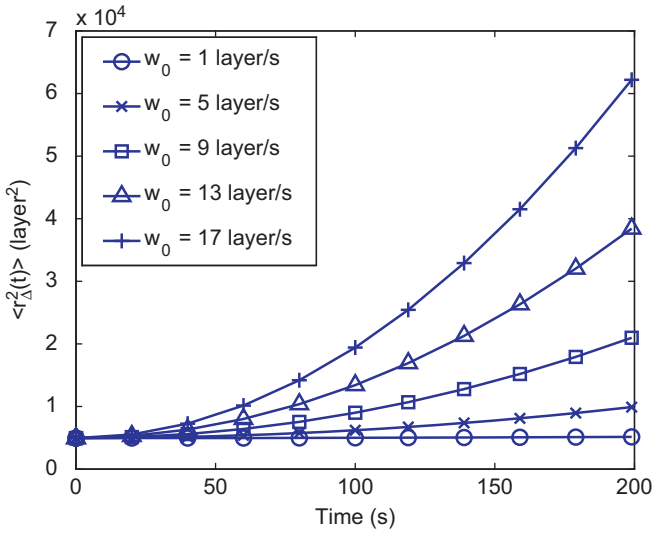

Fig. 10. Evolution of expected aggregate surface roughness with respect to time for different mean deposition rates (unit of w_0 is layer/s) obtained from kMC simulations. Patterned deposition with $k=1$, $P=8000$, $M=100$ layer/s and $A = 0.1w_0$.

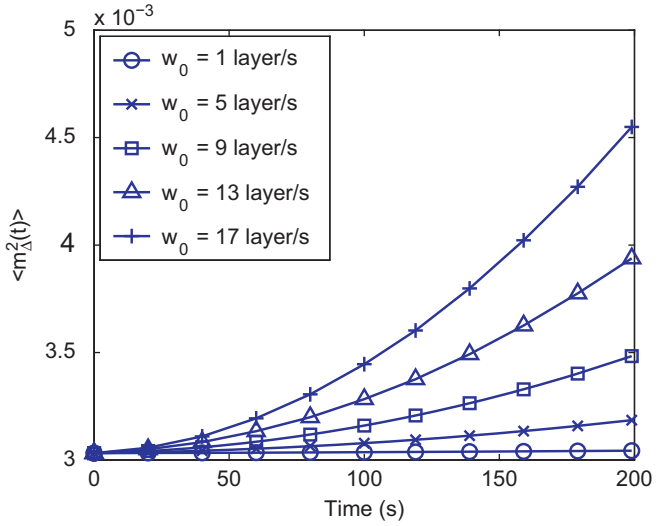

Fig. 11. Evolution of expected aggregate surface slope with respect to time for different mean deposition rates (unit of w_0 is layer/s) obtained from kMC simulations. Patterned deposition with $k=1$, $P=8000$, $M=100$ layer/s, $P=8000$, $M=100$ layer/s and $A = 0.1w_0$.

Figs. 10 and 11. The introduction of a patterned deposition rate profile significantly changes the dynamic profile of aggregate surface morphology, and the values of both aggregate roughness and slope increase by several orders of magnitude. Furthermore, simulations are carried out at $w_0 = 2$ layer/s with different magnitude, A, values to investigate the influence of the strength of patterned deposition on the evolution profiles of aggregate surface morphology. As shown in Figs. 12 and 13, the magnitude, A, has a substantial influence on the dynamics of aggregate surface morphology. Both aggregate roughness and aggregate slope can be increased substantially by manipulating A compared to the aggregate surface morphology achieved with a uniform deposition rate profile. Thus, the introduction of a patterned deposition rate profile, in conjunction with wafer grating, expands the range of surface morphology values that can be obtained and makes surface morphology control at length scales comparable to visible light wavelength possible. Finally, we note that in practice, there are a couple of standard ways to achieve wafer

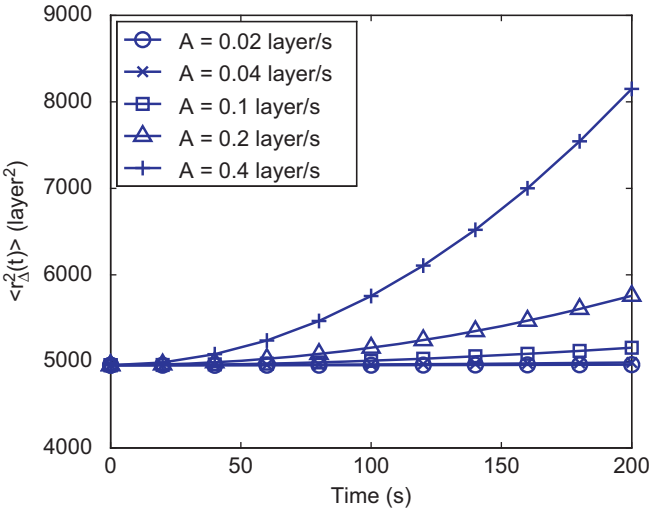

Fig. 12. Evolution of expected aggregate surface roughness with respect to time for different patterned deposition rate magnitudes obtained from kMC simulations. Patterned deposition with $k=1$, $P=8000$, $M=100$ layer/s and $w_0=2$ layer/s.

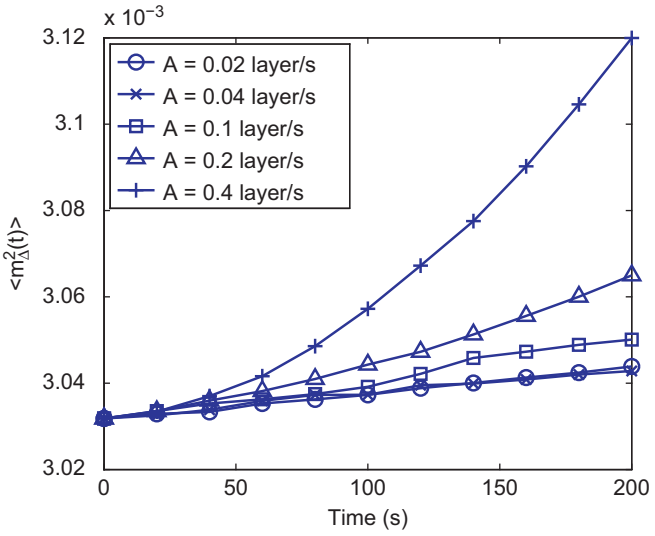

Fig. 13. Evolution of expected aggregate surface slope with respect to time for different patterned deposition rate magnitudes obtained from kMC simulations. Patterned deposition with $k=1$, $P=8000$, $M=100$ layer/s and $w_0=2$ layer/s.

grating (for example, line or sinusoidal grating), and this is normally done before the deposition process takes place. This is why the grating comes as an initial condition in the kMC and stochastic PDE models (see below) to capture the initial – grated – nature of the wafer. Grating parameters cannot play the role of manipulated variables like deposition rate and temperature because grating parameters cannot be manipulated (varied) in real-time.

3. Closed-form modeling and parameter estimation

3.1. Edward–Wilkinson-type equation of aggregate surface height

Given the complexity of the two species deposition process and the need to control surface roughness and slope at spatial scales comparable to the wavelength of visible light, the direct computation of a closed-form model describing the surface height evolution suitable for controller design, from the microscopic deposition mechanisms is a very difficult task. Therefore, a hybrid modeling approach should be used in which a basic closed-form modeling structure is first postulated and the model parameters are computed such that the predictions of key variables from the closed-form model are close to the one of the kinetic Monte-Carlo model for a broad set of operating conditions. It is well known that an Edward–Wilkinson (EW)-type equation, which is a second-order stochastic PDE, can be used in this case to describe and predict the aggregate surface height profile (Huang et al., 2011, 2012a) as follows:

$$\frac{\partial h_\Delta}{\partial t} = w(x,t) + c_2 \frac{\partial^2 h_\Delta}{\partial x^2} + \xi(x,t) \tag{9}$$

subject to the following periodic boundary conditions:

$$h_\Delta(0,t) = h_\Delta(L,t) \tag{10}$$

$$\frac{\partial h_\Delta}{\partial x}(0,t) = \frac{\partial h_\Delta}{\partial x}(L,t) \tag{11}$$

In this work, the use of a sinusoidal grated wafer introduces a non-zero initial condition, as follows:

$$h_\Delta(x,0) = h_\Delta^0(x) = M_\Delta \cdot \sin\left(\frac{2\pi x}{L}\right) + M_\Delta \tag{12}$$

where $h_\Delta(x,t)$ is the aggregate surface height, $x \in [0, L/\Delta]$ is the spatial coordinate and M_Δ is the magnitude of wafer grating at the aggregate length scale. $\xi(x,t)$ is a Gaussian white noise with zero mean and the following covariance:

$$\langle \xi(x,t)\xi(x',t') \rangle = \sigma^2 \delta(x-x')\delta(t-t') \tag{13}$$

where $\delta(\cdot)$ denotes the Dirac delta function. In Eq. (9), the parameters c_2 and σ^2 depend on the deposition rate $w(x,t)$ (Huang et al., 2012b) and their explicit form will be computed in Section 3.3. A patterned deposition rate profile (control actuation), $w(x,t)$, is used of the form

$$w(x,t) = w_0(t) + A(t) \sin\left(\frac{2k\pi}{L}x\right) \tag{14}$$

where $w_0(t)$ is the total mean deposition rate and $A(t)$ is the total magnitude of patterned deposition rate.

To analyze the dynamics and obtain a solution of the EW equation suitable for real-time controller calculations, we first consider the eigenvalue problem of the linear operator of Eq. (9) to obtain its eigenvalues and eigenfunctions. Then the aggregate surface height profile can be expanded in an infinite series in terms of the eigenfunctions times time-varying coefficients. Substituting this expansion into Eq. (9) and taking the inner product with the adjoint eigenfunctions, the stochastic PDE can be transformed into a system of infinite stochastic linear ordinary differential equations (ODEs) of the form

$$\frac{dz_{2,0}(t)}{dt} = w_{2,0} + \xi_{2,0}(t) \tag{15}$$

$$\frac{dz_{p,n}(t)}{dt} = w_{p,n} + \lambda_n z_{p,n} + \xi_{p,n}(t) \quad p = 1,2,\ n = 1,\ldots,\frac{L}{2\Delta} \tag{16}$$

where $\xi_{p,n}(t) = \int_0^L \xi(x,t)\phi_{p,n}(x)\,dx$ is the projection of the noise $\xi(x,t)$ on the ODE for $z_{p,n}$. The noise term, $\xi_{p,n}$, has zero mean and covariance

$$\langle \xi_{p,n}(t)\xi_{p,n}(t') \rangle = \sigma^2 \delta(t-t') \tag{17}$$

Similarly, $w_{p,n}$ is the projection of w on the ODE for $z_{p,n}(t)$, $w_{p,n} = \int_0^L \phi_{p,n}(x) w(x)\,dx$

- If $p=1$,

$$w_{1,n} = \begin{cases} 0, & n \neq k \\ A\sqrt{\frac{L}{2}}, & n = k \end{cases} \tag{18}$$

- If $p=2$,

$$w_{2,n}=\begin{cases}0, & n\neq 0\\ A\sqrt{L}, & n=0\end{cases} \tag{19}$$

The temporal evolution of the variance of mode $z_{p,n}$ can be obtained from the solution of the linear ODEs of Eqs. (15) and (16) as follows:

$$\langle z_{2,0}(t)\rangle = w_{2,0}(t-t_0) \tag{20}$$

$$\mathrm{var}(z_{2,0}(t)) = \sigma^2(t-t_0) \tag{21}$$

$$\langle z(t)\rangle = e^{\lambda(t-t_0)}\langle z(t_0)\rangle + \frac{w_p}{\lambda}(e^{\lambda(t-t_0)}-1) \tag{22}$$

$$\mathrm{var}(z(t)) = e^{2\lambda(t-t_0)}\mathrm{var}(z(t_0)) + \sigma^2\frac{e^{2\lambda(t-t_0)}-1}{2\lambda} \tag{23}$$

where $z(t)=z_{p,n}(t)$, $\lambda=\lambda_n$, $w_p=w_{p,n}$ for $n\neq 0$ and $z(t_0)=z_{p,n}(t_0)$ can be calculated as follows:

- If $p=1$,

$$z_{1,n}(t_0)=\begin{cases}0, & n\neq P\\ M_\Delta\sqrt{\frac{L}{2}}, & n=P\end{cases} \tag{24}$$

- If $p=2$,

$$z_{2,n}(t_0)=0 \tag{25}$$

For the details on how to solve Eq. (9), refer to Huang et al. (2012a).

3.2. Aggregate surface root–mean–square roughness and slope

Aggregate surface roughness of the thin film is defined as the standard deviation of the aggregate surface height profile from its average height

$$r_\Delta(t)=\sqrt{\frac{1}{L}\int_0^L [h_\Delta(x,t)-\bar{h}_\Delta(t)]^2\,dx} \tag{26}$$

where $\bar{h}_\Delta(t)=(1/L)\int_0^L h_\Delta(x,t)\,dx$ is the average aggregate surface height. It can be shown that (Huang et al., 2012a)

$$\langle r_\Delta^2(t)\rangle = \frac{1}{L}\sum_{n=1}^{L/(2\Delta)}(\langle z_{1,n}^2\rangle + \langle z_{2,n}^2\rangle) \tag{27}$$

where

$$\langle z_{p,n}^2\rangle = \mathrm{var}(z_{p,n}) + \langle z_{p,n}\rangle^2 \tag{28}$$

The expression of Eqs. (27)–(28), which is derived analytically, will be used in the MPC formulation; see Eq. (33) below.

Similarly, the aggregate RMS slope is defined as the root-mean-square of the aggregate surface slope in the x-direction as follows:

$$m_\Delta(t)=\sqrt{\frac{1}{L}\int_0^L\left(\frac{\partial h_\Delta}{\partial x}\right)^2 dx}=\sqrt{\frac{1}{L}\sum_{i=0}^{L/\Delta}\left(\frac{h_\Delta(i+1,t)-h_\Delta(i,t)}{\Delta}\right)^2\Delta} \tag{29}$$

It can be shown that (Huang et al., 2012a)

$$\langle m_\Delta^2(t)\rangle = \sum_{p=1}^{2}\sum_{n=0}^{L/(2\Delta)} K_{p,n}\langle z_{p,n}^2\rangle = \sum_{m=1}^{L/(2\Delta)}(K_{1,m}\langle z_{1,m}^2\rangle + K_{2,m}\langle z_{2,m}^2\rangle) \tag{30}$$

where

$$K_{p,n}=\frac{8}{L^2\Delta}\sin^2\left(\frac{\pi n}{L/\Delta}\right)\sum_{i=0}^{L/(2\Delta)}\left(\cos^2\left(\frac{n\pi}{L/\Delta}(2i+1)\right)\right)$$
$$=\begin{cases}\frac{8}{L\Delta^2}\sin^2\left(\frac{\pi n}{L/\Delta}\right) & n=0\\ \frac{4}{L\Delta^2}\sin^2\left(\frac{\pi n}{L/\Delta}\right) & n\neq 0\end{cases} \tag{31}$$

The expression of Eq. (30), which is derived analytically, will be used in the MPC formulation; see Eq. (33) below.

3.3. Parameter estimation

The two model parameters, c_2 and σ^2, in the EW equation of Eq. (9), can be determined as functions of the total mean deposition rate w_0 and of the total patterned deposition rate magnitude A. These parameters affect the dynamics of aggregate surface roughness and slope and can be estimated by fitting the predicted evolution profiles for aggregate surface roughness and slope from the EW equation to profiles of aggregate surface roughness and slope from kMC simulations. Least-square methods are used to estimate the model parameters so that the EW-model predictions are close in a least-square sense to the kMC simulation data. Comparison of the predictions of both models is shown in Fig. 14. Based on c_2 and σ^2 values obtained from these fitting results, two linear functions are chosen to estimate c_2 and σ^2 values at different w with the least-square method

$$c_2(w)=a_{c_2}\cdot w+b_{c_2}$$

$$\sigma^2=a_{\sigma^2}\cdot w+b_{\sigma^2} \tag{32}$$

where a_{c_2}, b_{c_2}, a_{σ^2} and b_{σ^2} are time-invariant fitting model parameters. The fitting results are shown in Figs. 15 and 16. To verify the fitting functions, two more groups of simulations were carried out with larger deposition rates ($w=17$ and 21 layer/s) and fitted to EW equation, and the obtained values for c_2 and σ^2 are used to extend the fitting curve to show the validity of the chosen fitting functions. It has been verified that fitting results based on kMC simulation with uniform deposition rate profiles ($A=0$) can be used to estimate c_2 and σ^2 values for simulations with spatially distributed deposition rate profiles (Huang et al., 2011), and this assumption is still used in this work.

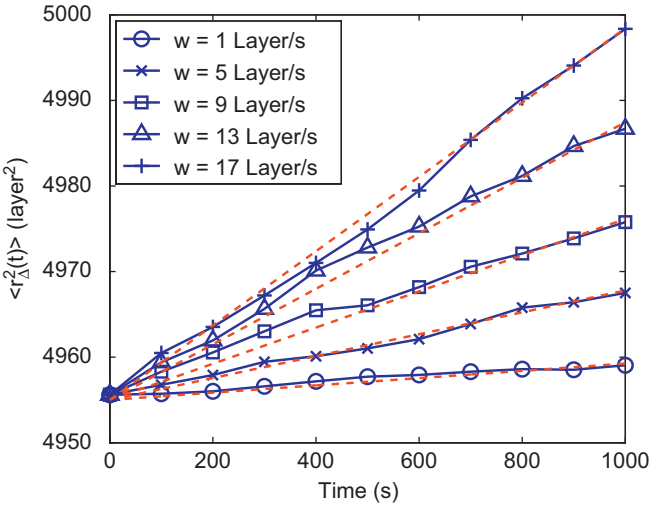

Fig. 14. Evolution of expected aggregate surface roughness with respect to time for different spatially uniform deposition rates obtained from kMC simulations (solid lines with symbols). The analytical solutions for the aggregate surface roughness obtained from the corresponding EW equations with the fitted values for c_2 and σ^2 are also shown (dashed lines).

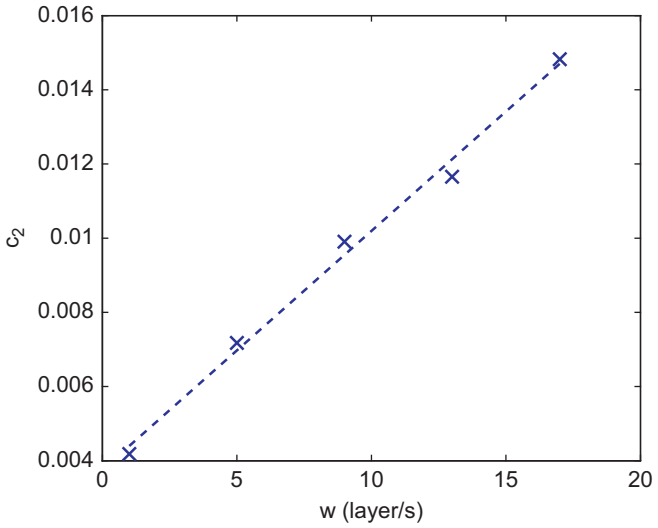

Fig. 15. c_2 values for different spatially uniform deposition rates w. The solid line is the result of a linear fitting function and it is the c_2 versus w relationship used by the predictive controller.

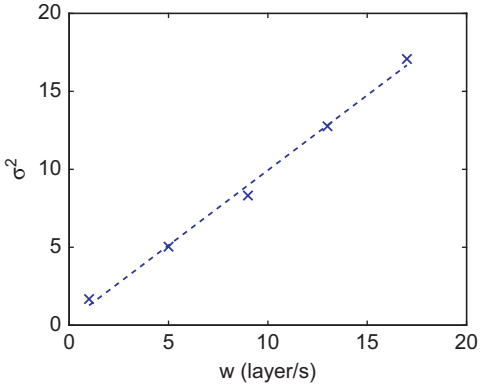

Fig. 16. σ^2 values for different spatially uniform deposition rates w. The solid line is the result of a linear fitting function.

4. Model predictive control

In this section, a model predictive controller is designed based on the dynamic models of aggregate surface roughness and slope to simultaneously control the expected values of aggregate surface roughness and slope square to desired levels. The dynamics of aggregate surface roughness and slope of the TCO layers are described by both the kMC model and the EW equation. State feedback control is considered in this work, and $h_\Delta(x,t)$ is assumed to be available for feedback. In practice, real-time surface height measurements can be obtained via atomic force microscopy (AFM) systems and can be used to compute the quantities – aggregate surface roughness and slope – used by the controller using Eqs. (27) and (30).

4.1. MPC formulation for regulation of aggregate roughness and slope

The control objective in this work is to regulate aggregate surface roughness and slope to desired levels within a model predictive control framework. Due to the stochastic nature of the variables, the expected values of aggregate surface roughness and slope, $\langle r_\Delta^2(t)\rangle$ and $\langle m_\Delta^2(t)\rangle$, are chosen as the control objectives. The total mean deposition rate, w_0 ($w_0 = w_{1,0}+w_{2,0}$), and magnitude of patterned deposition rate, A ($A = A_1+A_2$), are chosen as the manipulated inputs; the substrate temperature is fixed at $T=800$ K during all closed-loop simulations. To account for a number of practical considerations, several constraints are added to the control problem. In particular, since $w(x)\geq 0$, the constraints $0\leq A_1\leq w_{1,0}$ and $0\leq A_2\leq w_{2,0}$ are imposed to ensure $w(x,t)>0$, $\forall(x,t)$. To ensure the validity of the closed-form process model, there is a constraint on the range of variation of the mean deposition rate. Another constraint is imposed on the rate of change of the mean deposition rate to account for actuator limitations. The control action at time t is obtained by solving a finite-horizon optimal control problem. The cost function in the optimal control problem includes penalty on both aggregate roughness and slope with independent weighting factors. Since the dynamics of aggregate surface roughness and slope are different by several orders of magnitude, relative deviations are used in the formulation of the cost function to make the magnitude of these two terms comparable in the cost function. The optimization problem is subject to the dynamics of the aggregate surface height of Eq. (9), which account for wafer grating. Specifically, the MPC problem at time t is formulated as follows:

$$\min_{w_0,A} f(w_0,A) = q_{r^2}\left[\frac{r_{set}^2-\langle r_\Delta^2(t_f)\rangle}{r_{set}^2}\right]^2 + q_{m^2}\left[\frac{m_{set}^2-\langle m_\Delta^2(t_f)\rangle}{m_{set}^2}\right]^2 \tag{33}$$

where

$$\langle r_\Delta^2(t_f)\rangle = \frac{1}{L}\sum_{n=1}^{L/(2\Delta)}\sum_{p=1}^{2}\langle z_{p,n}^2(t_f)\rangle$$

$$\langle m_\Delta^2(t_f)\rangle = \sum_{n=1}^{L/(2\Delta)}\sum_{p=1}^{2}(K_{p,n}\langle z_{p,n}^2(t_f)\rangle) \tag{34}$$

$$\langle z_{p,n}^2(t_f)\rangle = \mathrm{var}(z_{p,n}(t_f)) + \langle z_{p,n}(t_f)\rangle^2 \tag{35}$$

$$\langle z_{p,n}(t_f)\rangle = e^{\lambda_n(t_f-t)}\langle z_{p,n}(t)\rangle + \frac{w_p}{\lambda_n}(e^{\lambda_n(t_f-t)}-1) \tag{36}$$

$$\mathrm{var}(z_{p,n}(t_f)) = e^{2\lambda_n(t_f-t)}\mathrm{var}(z_{p,n}(t)) + \sigma^2(w)\frac{e^{2\lambda_n(t_f-t)}-1}{2\lambda_n} \tag{37}$$

$$\lambda_n = -\frac{4c_2(w)\pi^2}{L^2}n^2 \tag{38}$$

and

$$c_2(w_0) = a_{c_2}\cdot w_0 + b_{c_2} \tag{39}$$

$$\sigma^2(w_0) = a_{\sigma^2}\cdot w_0 + b_{\sigma^2} \tag{40}$$

subject to:

$$w_{\min}\leq w_0\leq w_{\max},\quad |w_0(t)-w_0(t-dt)|\leq \delta w_{\max} \tag{41}$$

where t is the current time, dt is the sampling time, q_{r^2} and q_{m^2} are the weighting penalty factors for the deviations of $\langle r_\Delta^2\rangle$ and $\langle m_\Delta^2\rangle$ from their respective set-points at the ith prediction step, $w_{\min}$ and $w_{\max}$ are the lower and upper bounds on the mean deposition rate, respectively, and $\delta w_{\max}$ is the limit on the rate of change of the mean deposition rate. Due to the influence of wafer grating, $z_{p,n}(t_0)$ follows Eqs. (24) and (25). The prediction horizon is the interval from the current time t to the end of the deposition time t_f (the subscript f stands for final time) and the control horizon is one, meaning a pair (w_0,A) is computed at each time t.

The optimal control actions are obtained from the solution of the multivariable optimization problem of Eq. (33) and are applied to the deposition process model over dt (i.e., either the EW equation model or the kMC model) during the time interval $(t,t+dt)$. At time $t+dt$, a new measurement of aggregate surface roughness and slope is received by the controller and the MPC

problem of Eq. (33) is solved for the next set of control actions. An interior point method optimizer, IPOPT (Wächter and Biegler, 2006), is used to solve the optimization problem in the MPC formulation. The stability of the closed-loop system is inherently guaranteed by the negative values of all the eigenvalues of the spatial differential operator of Eq. (9) used to describe the dynamics of surface height profiles.

5. Simulation results

In this section, the model predictive controller of Eq. (33) is applied to both the one-dimensional EW equation type model of Eq. (9) and the one-dimensional kMC model of the thin film growth process. The sinusoidal grated wafer period is 8000, the grating magnitude is 100 layers, the mean deposition rate ranges from 0.1 to 10 layer/s, the substrate temperature is fixed at 800 K, the lattice size of the kMC model is fixed at 40,000 sites, the aggregation size is fixed at 400 to make the results relevant to thin film solar cell applications and five sine waves are used in the patterned deposition rate profile. The sampling time is 10 s; this sampling time is enough for the MPC to carry out the calculations needed to compute the control action. In addition to the deposition rate, the temperature may be used as a manipulated input but it should vary in space to induce substantial aggregate surface roughness and slope values at spatial scales comparable to the visible light wavelength. Each closed-loop simulation lasts for 200 s. Expected values are calculated from 10 independent closed-loop system simulation runs; further increase of the number of independent simulations did not appreciably change the computed expected values. In all the simulations, the aggregate surface roughness and slope set-points remain the same, specifically, $r^2_{set}=5500$ and $m^2_{set}=0.005$.

5.1. MPC application to EW equation model

In this subsection, the EW equation model is utilized in the closed-loop control problem as the plant model. First, the problem of regulating aggregate surface roughness is considered. In this problem, the cost function includes only penalty on the deviation of the expected aggregate surface roughness square from its set-point, i.e., $q_{r^2}=1$ and $q_{m^2}=0$. Fig. 17 shows the evolution profile of $\langle r^2_\Delta(t)\rangle$ under the model predictive controller of Eq. (33). It is clear that the controller drives the expected aggregate surface roughness to its set-point at the end of the simulation. Fig. 18 shows the input profiles of w_0 and A for these simulations.

Next, the aggregate surface slope is regulated. In this case, the cost function includes only penalty on the deviation of the expected value of aggregate surface slope square from its set-point ($q_{m^2}=1$, $q_{r^2}=0$). Fig. 19 shows the evolution profile of the expected aggregate slope square. The aggregate slope reaches its set-point at t_f=200 s. Fig. 20 displays the input profile in this scenario.

5.2. MPC application to kMC model

In this subsection, the kMC model is used in the closed-loop control problem as the plant model, while all the other settings remain the same. Fig. 21 shows the aggregate surface roughness in the case of roughness-only control and its corresponding

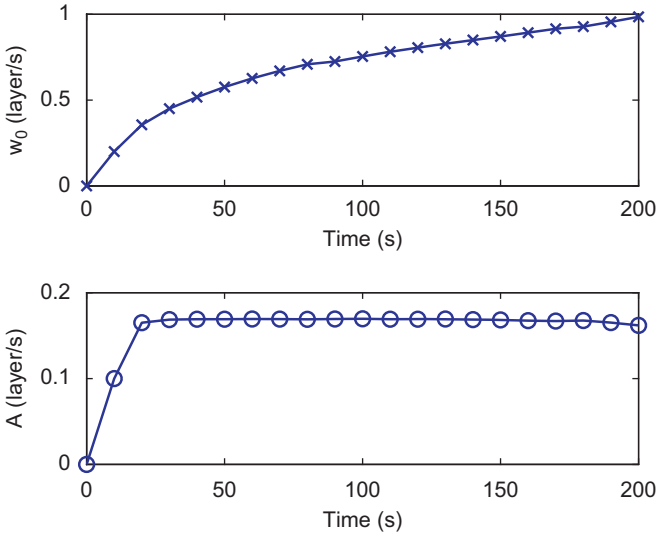

Fig. 18. Input profiles for aggregate roughness-only control problem with EW equation as the plant model. $q_{r^2}=1$, $q_{m^2}=0$ and $r^2_{set}=5500$.

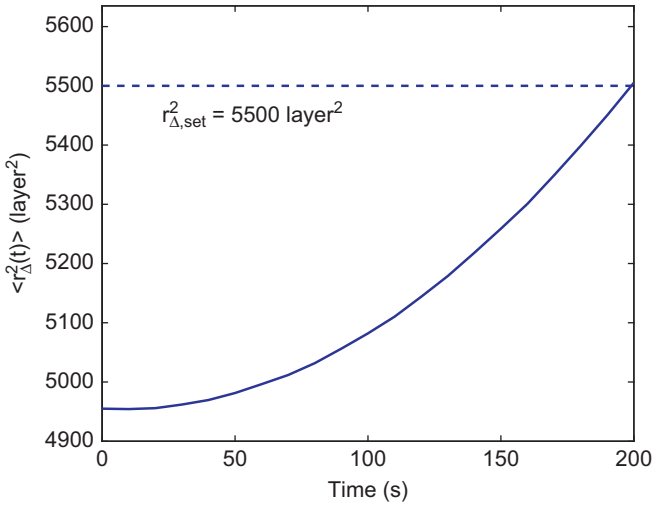

Fig. 17. Profile of expected aggregate surface roughness square with EW equation as the plant model. $q_{r^2}=1$, $q_{m^2}=0$ and $r^2_{set}=5500$.

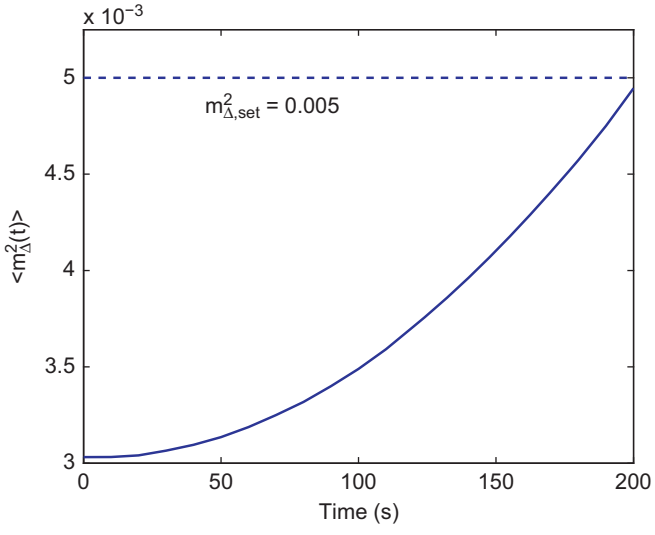

Fig. 19. Profile of expected aggregate surface slope square with EW equation as the plant model. $q_{r^2}=0$, $q_{m^2}=1$ and $m^2_{set}=0.005$.

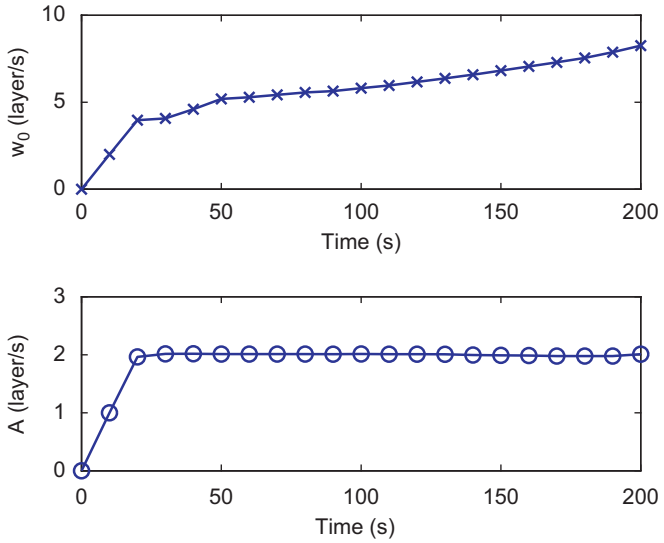

Fig. 20. Input profiles for aggregate slope-only control problem with EW equation as the plant model. $q_{r^2}=0$, $q_{m^2}=1$ and $m^2_{set}=0.005$.

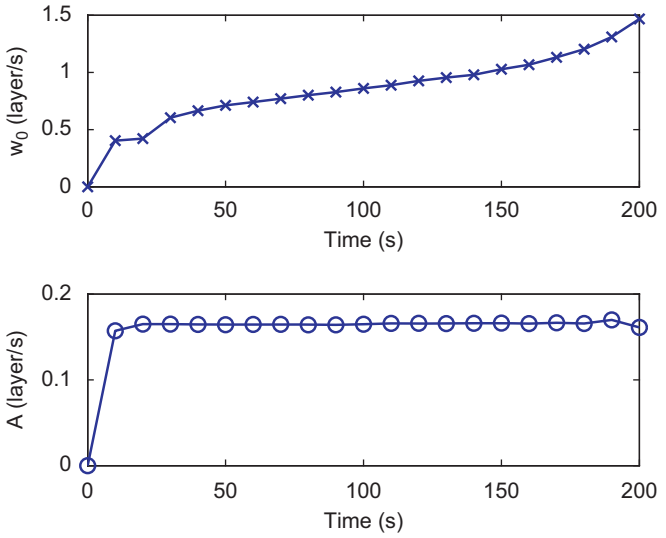

Fig. 22. Input profiles for aggregate roughness-only control problem with kMC model as the plant model. $q_{r^2}=1$, $q_{m^2}=0$ and $r^2_{set}=5500$.

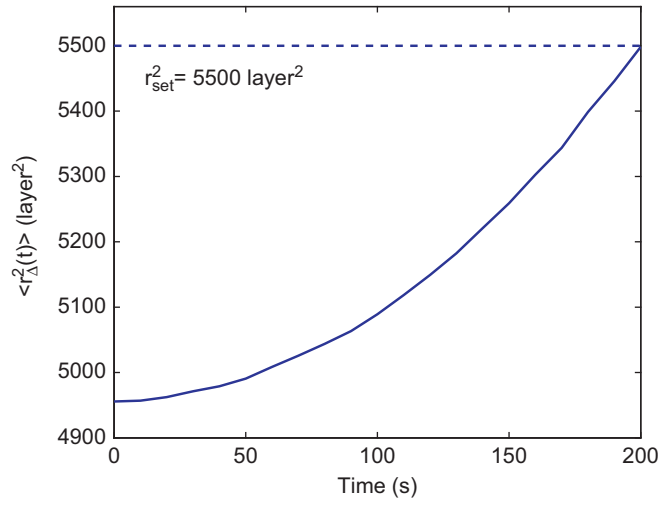

Fig. 21. Profile of expected aggregate surface roughness square with kMC model as the plant model. $q_{r^2}=1$, $q_{m^2}=0$ and $r^2_{set}=5500$.

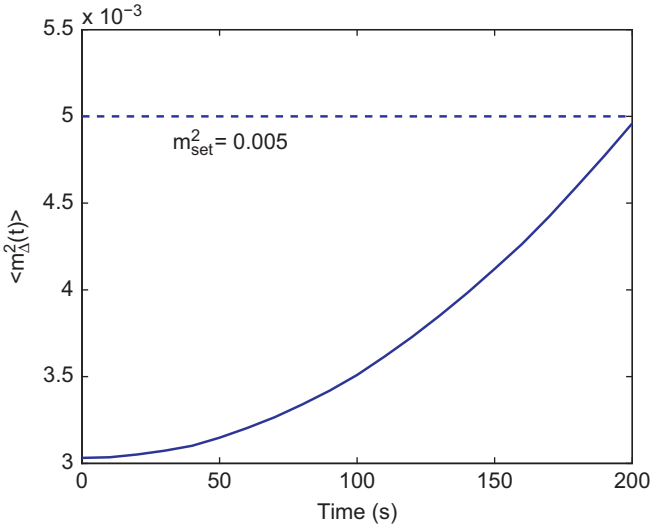

Fig. 23. Profile of expected aggregate surface slope square with kMC model as the plant model. $q_{r^2}=0$, $q_{m^2}=1$ and $m^2_{set}=0.005$.

manipulated input profiles are shown in Fig. 22, while Fig. 23 shows the aggregate surface slope in the case of slope-only control and its corresponding manipulated input profiles are shown in Fig. 24. In both conditions, we see that both aggregate roughness and slope successfully reach their set-points at the end of the simulations (t_f=200 s). Furthermore, the closed-loop evolution profiles with kMC as the plant model are very similar to the closed-loop profiles that use the EW equation as the plant model, which implies that the EW equation model used in this work can accurately predict the kMC simulation results.

Simultaneous regulation of aggregate surface roughness and slope has also been investigated. Similar to the case where the EW equation is used as the plant model, the weighting factor of aggregate slope square, q_{r^2}, is kept at 1, and the weighting factor of aggregate roughness square, q_{m^2}, ranges from 10^{-2} to 10^{7}. Fig. 25 shows the values of expected aggregate roughness and slope at the end of simulations as a function of q_{m^2}/q_{r^2}. It can be seen that the expected value of aggregate roughness approaches its set-point as q_{m^2} increases at the cost of larger deviation of the aggregate slope from its set-point.

6. Conclusions

In this work, a two species thin film deposition process is simulated via a kinetic Monte-Carlo method on a sinusoidal grated square lattice (L=40,000) with different growth mechanisms for each species. Investigation of the simulation dynamics indicates the necessity of using a patterned deposition rate profile in the deposition to generate significant aggregate surface roughness and slope to achieve desired solar cell performance. An Edwards–Wilkinson-type equation for the aggregate surface profile is used to predict the surface temporal evolution of aggregate surface roughness and slope. A model predictive controller is designed to regulate aggregate surface roughness and slope to desired levels, and the controller is applied to both the EW equation and the kMC model. Simulation results demonstrate the

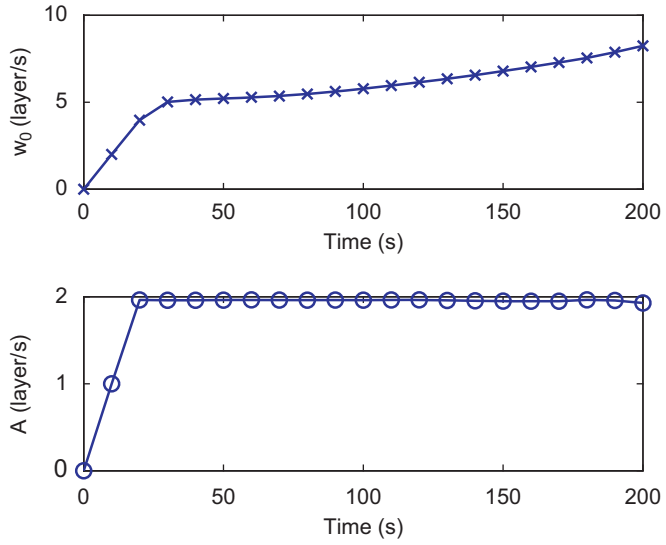

Fig. 24. Input profiles for aggregate slope-only control problem with kMC model as the plant model. $q_{r^2}=0$, $q_{m^2}=1$ and $r^2_{set}=0.005$.

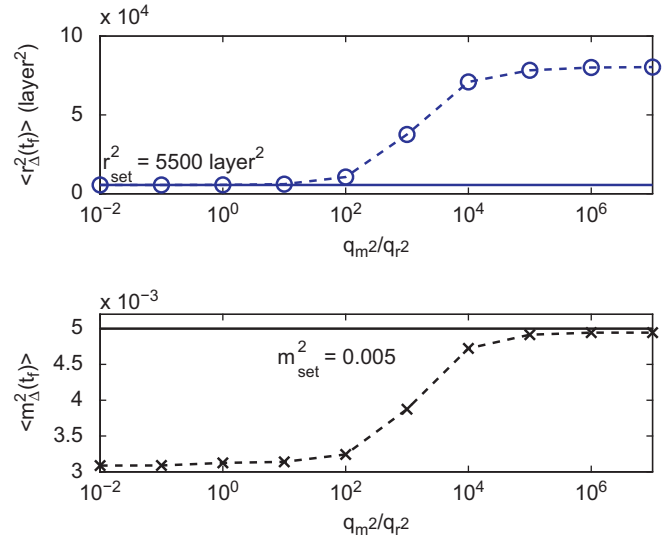

Fig. 25. $\langle r^2_{\Delta}(t_f)\rangle$ and $\langle m^2_{\Delta}(t_f)\rangle$ at the end of closed-loop simulations (t_f=200 s) for different penalty weighting factors in the predictive controller with kMC model as the plant model. $10^{-2}\le q_{m^2}\le 10^{7}$, $q_{r^2}=1$, $r^2_{set}=5500$ and $m^2_{set}=0.005$.

applicability and effectiveness of the controller to regulate the surface morphology on a sinusoidal grated wafer.

Acknowledgment

Financial support from the National Science Foundation, CBET-0652131, and a UCLA Doctoral Dissertation Year Fellowship for Jianqiao Huang, are gratefully acknowledged.

References

Campa, A., Isabella, O., Van Erven, R., Peeters, P., Borg, H., Krc, J., Topic, M., Zeman, M., 2010. Optimal design of periodic surface texture for thin-film α-Si : h solar cells. Prog. Photovolt. 18, 160–167.

Chen, J., Wang, Q., Li, H., 2010. Microstructured design of metallic diffraction gratings for light trapping in thin-film silicon solar cells. Opt. Commun. 283, 5236–5244.

Chong, T., Wilson, J., Mokkapati, S., Catchpole, K.R., 2012. Optimal wavelength scale diffraction gratings for light trapping in solar cells. J. Opt. 14, 024012–024020.

Christofides, P.D., Armaou, A., Lou, Y., Varshney, A., 2008. Control and Optimization of Multiscale Process Systems. Birkhäuser, Boston.

Das, R., Jana, T., Ray, S., 2005. Degradation studies of transparent conducting oxide: a substrate for microcrystalline silicon thin film solar cells. Solar Energy Mater. Solar Cells 86, 207–216.

Ferry, V., Polman, A., Atwater, H., 2011. Modeling light trapping in nanostructured solar cells. ACS Nano 5, 10055–10064.

Gospodyn, J., Sit, J.C., 2006. Characterization of dielectric columnar thin films by variable angle Mueller matrix and spectroscopic ellipsometry. Opt. Mater. 29, 318–325.

Green, M.A., 2007. Thin-film solar cells: review of materials, technologies and commercial status. J. Mater. Sci. Mater. Electron. 18, 15–19.

Hu, G., Huang, J., Orkoulas, G., Christofides, P.D., 2009a. Investigation of film surface roughness and porosity dependence on lattice size in a porous thin film deposition process. Phys. Rev. E 80, 041122.

Hu, G., Orkoulas, G., Christofides, P.D., 2009b. Modeling and control of film porosity in thin film deposition. Chem. Eng. Sci. 64, 3668–3682.

Huang, J., Hu, G., Orkoulas, G., Christofides, P., 2010a. Dependence of film surface roughness and slope on surface migration and lattice size in thin film deposition processes. Chem. Eng. Sci. 65, 6101–6111.

Huang, J., Hu, G., Orkoulas, G., Christofides, P.D., 2011b. Dynamics and lattice-size dependence of surface mean slope in thin-film deposition. Ind. Eng. Chem. Res. 50, 1219–1230.

Huang, J., Orkoulas, G., Christofides, P.D., 2012a. Modeling and control of transparent conducting oxide layer surface morphology for improved light trapping. Chem. Eng. Sci. 74, 135–147.

Huang, J., Orkoulas, G., Christofides, P.D., 2012b. Simulation and control of aggregate surface morphology in a two-stage thin film deposition process for improved light trapping. Chem. Eng. Sci. 71, 520–530.

Huang, J., Zhang, X., Orkoulas, G., Christofides, P.D., 2011. Dynamics and control of aggregate thin film surface morphology for improved light trapping: implementation on a large-lattice kinetic Monte Carlo model. Chem. Eng. Sci. 66, 5955–5967.

Krč, J., Zeman, M., 2003. Effect of surface roughness of ZnO:Al films on light scattering in hydrogenated amorphous silicon solar cells. Thin Solid Films 426, 296–304.

Levine, S.W., Clancy, P., 2000. A simple model for the growth of polycrystalline Si using the kinetic Monte Carlo simulation. Model. Simul. Mater. Sci. Eng. 8, 751–762.

Levine, S.W., Engstrom, J.R., Clancy, P., 1998. A kinetic Monte Carlo study of the growth of Si on Si(100) at varying angles of incident deposition. Surf. Sci. 401, 112–123.

Li, H., Wang, Q., Chen, J., Krc, J., Soppe, W., 2012. Light trapping in amorphous silicon solar cells with periodic grating structures. Opt. Commun. 285, 808–815.

Madzharov, D., Dewan, R., Knipp, D., 2011. Influence of front and back grating on light trapping in microcrystalline thin-film silicon solar cells. Opt. Express 19, A95–A107.

Mirica, E., Kowach, G., Evans, P., Du, H., 2004. Morphological evolution of ZnO thin films deposited by reactive sputtering. Cryst. Growth Des. 4, 147–156.

Moller, S., Palumbo, R., 2001. Solar thermal decomposition kinetics of ZnO in the temperature range 1950–2400 k. Chem. Eng. Sci. 56, 4505–4515.

Muller, J., Rech, B., 2004. TCO and light trapping in silicon thin film solar cells. Solar Energy 77, 917–930.

Naqavi, A., Soderstrom, K., Haug, F.J., Paeder, V., Scharf, T., Herzig, H.P., Ballif, C., 2011. Enhanced light trapping in realistic thin film solar cells using one-dimensional gratings. Proc. SPIE Int. Soc. Opt. Eng. 8065, 80650–80657.

Ni, D., Christofides, P.D., 2005. Multivariable predictive control of thin film deposition using a stochastic PDE model. Ind. Eng. Chem. Res. 44, 2416–2427.

Poruba, A., Fejfar, A., Remeš, Z., Špringer, J., Vaněček, M., Kočka, J., 2000. Optical absorption and light scattering in microcrystalline silicon thin films and solar cells. J. Appl. Phys. 88, 148–160.

Rowlands, S.F., Livingstone, J., Lund, C.P., 2004. Optical modelling of thin film solar cells with textured interface using the effective medium approximation. Solar Energy 76, 301–307.

van Sark, W., Brandsen, G.W., Fleuster, M., Hekkert, M.P., 2007. Analysis of the silicon market: will thin films profit? Energy Policy 35, 3125–3221.

Varshney, A., Armaou, A., 2005. Multiscale optimization using hybrid PDE/kMC process systems with application to thin film growth. Chem. Eng. Sci. 60, 6780–6794.

Varshney, A., Armaou, A., 2006. Optimal operation of GaN thin-film epitaxy employing control vector parametrization. AIChE J. 52, 1378–1391.

Wächter, A., Biegler, L.T., 2006. On the implementation of an interior-point filter line-search algorithm for large-scale nonlinear programming. Math. Program. 106 (1), 25–57.

Wang, L., Clancy, P., 2001. Kinetic Monte Carlo simulation of the growth of polycrystalline Cu films. Surface Sci. 473, 25–38.

Yang, Y.G., Johnson, R.A., Wadley, H.N., 1997. A Monte Carlo simulation of the physical vapor deposition of nickel. Acta Mater. 45, 1455–1468.

Zeman, M., Vanswaaij, R., 2000. Optical modeling of α-Si:H solar cells with rough interfaces: effect of back contact and interface roughness. J. Appl. Phys. 88, 6436–6443.